Factory acceptance of the Automated Alignment System for the Magdalena Ridge Observatory Interferometer

James J. D. Luis[a], David F. Buscher[a], Michelle J. Creech-Eakman[b], Christopher A. Haniff[a], Chris Salcido[b], Xiaowei Sun[a], and John S. Young[a]

[a]Cavendish Laboratory, University of Cambridge, J J Thomson Avenue, Cambridge, United Kingdom
[b]Magdalena Ridge Observatory, New Mexico Institute of Mining and Technology, 801 Leroy Pl, Socorro, New Mexico, United States

ABSTRACT

The Magdalena Ridge Observatory Interferometer (MROI) will soon incorporate an Automated Alignment System (AAS) to help limit visibility losses due to beam misalignment to ∼1%. This paper focuses on two key AAS components: (1) a dual-wavelength beacon at each unit telescope and (2) a detector for measuring the shear and tilt of beams of light arriving from the telescopes in the beam combining laboratory. We share initial results of acceptance tests for these components. Finally, we outline a plan for fully validating their performance against a list of derived requirements.

Keywords: beam alignment, Shack-Hartmann, beacon, tilt, shear, active optics, optical interferometry, MROI

1. INTRODUCTION

Optical interferometers typically relay beams of starlight from their unit telescopes to beam combining instruments in a laboratory via delay lines and beam reducing telescopes. Spatial information is inferred about the source by measuring the visiblity of fringes formed by interfering light collected by multiple telescopes. Fringe visibility is lost in interferometric measurements if the input beams become misaligned from each other in angle (tilt) or position (shear). Consider the example of a relative tilt misalignment between the beams in a free-space image plane beam combiner. In this class of combiners, the beams are focused onto a common point on a focal plane array. Ideally, all the focal spots overlap perfectly with each other. If a relative tilt develops between the beams due to misalignment, their focal spots lose perfect overlap. Since the intensity distribution of each spot is an Airy disk (i.e. non-uniform), the intensity of each beam is no longer equal at each point on the detector plane. The mismatch in intensity reduces the fringe visibility measured at each point on the detector. Fiber-fed combiners suffer similarly from imperfect alignment. The input beams must be focussed onto a set of fiber tips. If one beam is tilted away from the optical axis, its focal spot becomes offset from the core of the fiber, leading to a drop in coupling efficiency. When the light is combined with that from another channel that has not suffered misalignment, the resulting mismatch in their intensities drives a fall in measured visibility. It turns out that even small amounts of misalignment cause significant visibility loss. For free-space image plane combination, a differential tilt between two beams of 10 milliarcseconds (∼1″ in the beam combining laboratory at the MROI) causes a drop of order 1%, while a shear offset of 1% of the beam diameter likewise causes a visibility drop of 1%. This point can be demonstrated using physical optics simulations[1,2] in which pairs of beams are combined. Figures 1a and 1b plot the visibilities measured from these simulations. The former explores tilt misalignment in an image plane combiner, while the latter investigates shear misalignment in a multi-axial pupil plane combiner.

This paper starts by describing how the problem of beam alignment will be tackled at the Magdalena Ridge Observatory Interferometer (MROI) with an Automated Alignment System (AAS). We will outline up-to-date alignment schemes, requirements and component designs that have progressed since this system was described

---

Further author information: (Send correspondence to J. J. D. Luis)
E-mail: jjdl3@cam.ac.uk, Telephone: +44 1223 337 137

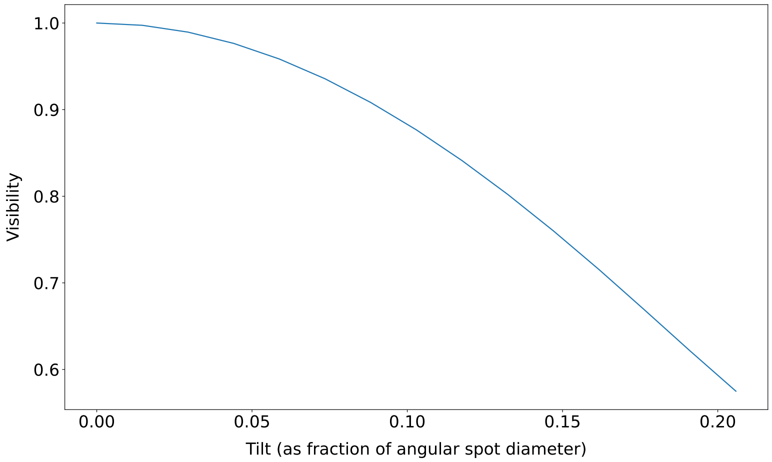

(a) Visibility loss as a function of differential tilt of the input beams for a two-beam image plane combiner.

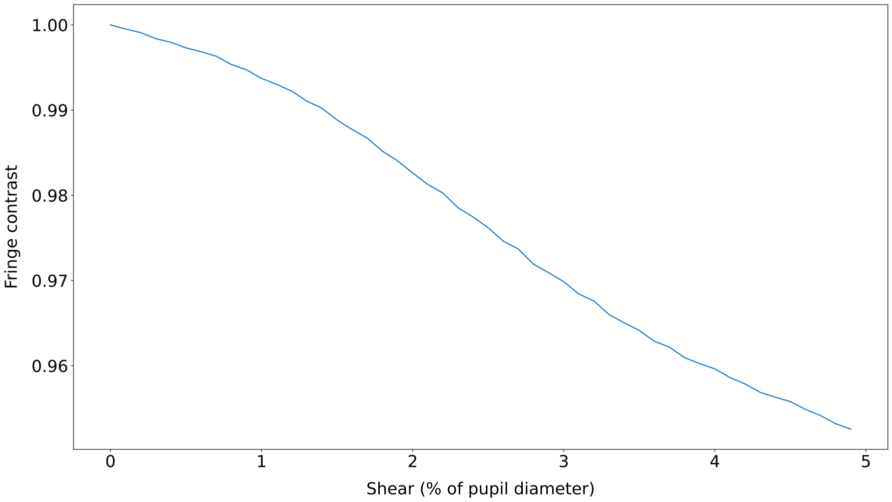

(b) Visibility loss as a function of diffferential beam shear for a multi-axial pupil plane combiner.

Figure 1: Measured visibility as a function of the relative beam misalignment for two types of beam combiner. These results were obtained by adding the appropriate electric field distributions in a physical optics simulation and computing the Fourier amplitude of the resulting spatially-encoded fringes.

at SPIE meetings in 2018[3] and 2020.[4] We then report on several results of performance verification experiments for the two most important hardware components of the AAS. Finally we summarise near term plans for their remaining factory acceptance tests.

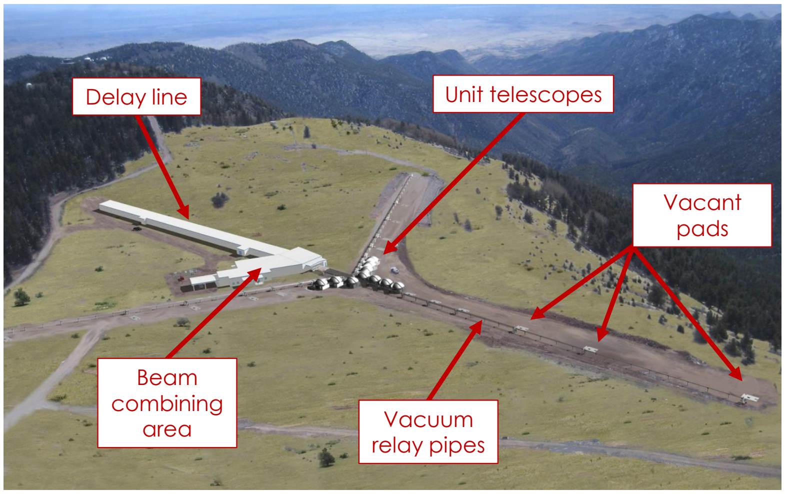

Figure 2: Artist's impression of the completed MROI site containing ten unit telescopes in their most compact arrangement.

2. BEAM ALIGNMENT AT THE MAGDALENA RIDGE OBSERVATORY INTERFEROMETER

2.1 Single beamline

The Magdalena Ridge Observatory Interferometer, under construction in New Mexico, USA, is a partnership between New Mexico Tech and the University of Cambridge, UK.[5] Its design includes ten 1.4 m-diameter relocatable unit telescopes(UTs) in the Y-shaped arrangement shown in Figure 2. The MROI will incorporate baselines from 7.8 m to 347 m and will operate initially at wavelengths between 0.6 µm and 2.4 µm. Its vacuum delay lines will provide up to 380 m of optical path compensation in a single stroke. At the time of writing, the first telescope is integrated at the apex of the array and is serviced by a vacuum beam relay of length ∼40 m, a 95 m long delay line (i.e. optical path difference up to 190 m) and a 7.3× reflective beam compressor in the beam combining laboratory. A second telescope is due to arrive towards the end of 2022. A set of optical tables has been installed that will allow the beam combining laboratory to be populated with beam alignment hardware, switchyard optics and the first light beam combiner.[6] A single beam train at the MROI can be considered as being comprised of three optical "entities" each with a "fixed" optical axis connected by adjustable beam relay mirror pairs, as shown in Figure 3:

- Entity 1: Unit telescope
- Entity 2: Delay line and beam compressor
- Entity 3: Beam combiner

The pairs of steerable mirrors provide the interfaces between the three optical axes and allow for management of tilt and shear of the propagating light. The optics on the left hand side of Figure 3 pass a beam that is 95 mm in diameter, while those on the right hand side of the figure handle the reduced beam diameter of 13 mm. The optics are likewise separated by their local environments. Optics on the left hand side of Figure 3 are generally exposed to outdoor temperatures that vary by ∼10 °C overnight while optics on the right hand side are kept in a much more stable environment where nightly variations are typically ≤0.2 °C. We expect therefore that beam alignment drifts on daily to weekly timescales will be overwhelmingly driven by thermal cycling of components located in the 95 mm space.

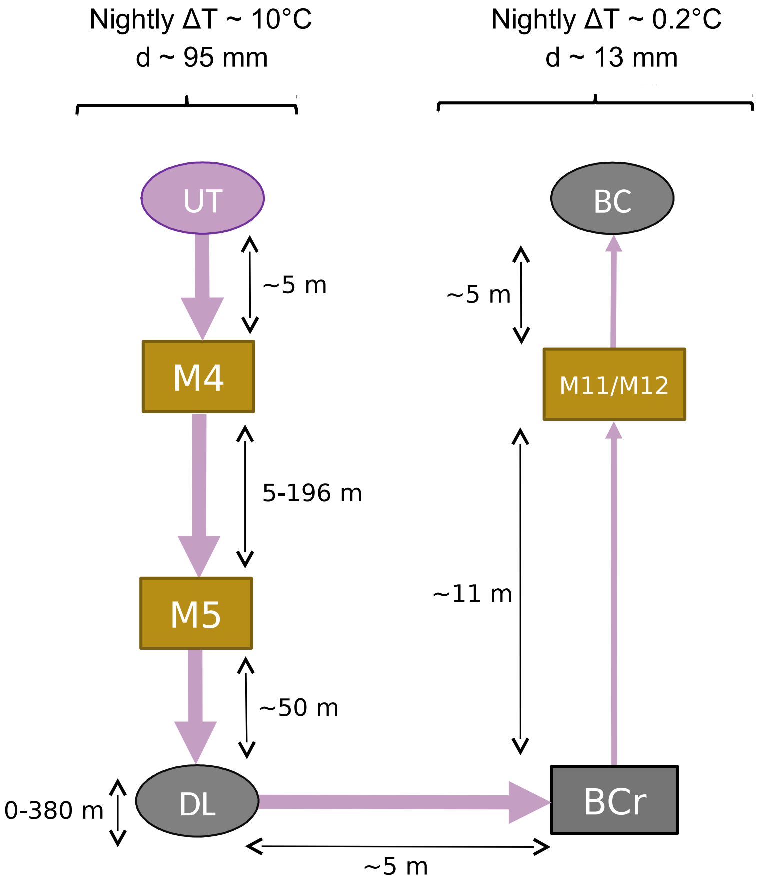

Figure 3: A single MROI beamline represented as a block diagram, consisting of three entities with associated optical axes: the Unit Telescope (UT), Delay Line (DL) / Beam compressor (BCr) and the Beam Combiner (BC). M4/M5 and M11/M12 are pairs of beam steering mirrors that interface these three axes in tilt and shear. Components on the left hand side transport a stellar beam that is nominally 95 mm in diameter while those on the right hand side transport a beam of 13 mm. Optics in the 95 mm space are generally exposed to outdoor temperature swings (the DL is an exception because it resides inside a building that shields it from large fluctuations), while those in the 13 mm space are housed in a passively temperature-stabilised laboratory. Typical distances between the optical elements are shown in metres.

2.2 Beam alignment requirements

The MROI optical error budget attempts to account for all effects that would degrade the signal-to-noise ratio of interferometric measurements made by the interferometer. Accordingly, it includes the following requirements relating to beam alignment errors:

- At the end of start-of-night alignment procedures, each beamline must be coaxial with the nominal optical axis within 15 mas in angle (on-sky) and within 0.9% of the pupil diameter in position.
- During the night the alignment of each beamline must not stray by more than 15 mas in angle (on-sky) and 1.4% of the pupil diameter in position.

An Automated Alignment System (AAS) has been proposed to satisfy these requirements while:

- Consuming no longer than 1 hour prior to the start of observing.
- Consuming no longer than 5 minutes per hour of observing time.
- Drawing no more than 3% of flux from the light passing to the beam combiners, averaged over each of the R, I, J, H and K bands.

2.3 Automated alignment system

The locations of the hardware elements of the Automated Alignment System (AAS) are shown, together with the other components of a single beamline in Figure 4. The AAS is comprised of six core elements. These are:

- **Unit Telescope Light Injection System, UTLIS** – A dual-wavelength collimated beacon at each Unit Telescope (UT) that is assured to be parallel to the stellar beam by setting its angle to be the servo fiducial for the UT's Fast-Tip Tilt (FTT) correction. The design and initial testing of this component is described in more detail in this paper (see Section 3).

- **Magic Optical Box, MOB** – A collimated light source in the beam combining laboratory that comprises a narrowband and a broadband source. The former is used for coarse alignment, while the latter is intended for fine alignment and piston equalisation between different beam lines. It is a single source whose light is split between the ten beamlines of the interferometer.

- **Large aperture photovoltaic quad cells, QC** – Coarse beam position sensors located in the vacuum pipes that are flipped in and out of the optical train on command. They sense the position of a beam up to 50 mm in diameter with resolution better than 100 µm.

- **Localised temperature sensors** – Thermocouples attached at various points on and around the beam relay mirrors M4 and M5 to sense temperature drifts and predict beam alignment drifts independently from any optical interrogation.

- **Back-End Active Stabilisation of Shear and Tilt, BEASST** – A Shack-Hartmann sensor in the beam combining laboratory that measures the shear and tilt of an incoming light beam from an artificial or stellar source. There will be one BEASST detector per beamline. The design and initial testing of this component is described in more detail in this paper (see Section 4).

- **Beam combiner alignment cameras** – While BEASST measures tilt and shear referenced to an optical axis, these alignment cameras will measure the tilt and shear of the beams entering a combiner relative to each other. The exact implementation varies by beam combiner. For example, the fringe tracker (ICONN[7]) passes combined beam pairs to a BEASST-like detector that measures shear and tilt simultaneously. The two beams are blocked sequentially so that only one beam is interrogated at a time. On the other hand the first light science combiner (FOURIER[6]) measures shear and tilt separately for its three input beams. To determine shear, just prior to entering the combiner each beam is deflected one at a time towards a shear-measuring camera. To determine tilt, the position of each beam at the image plane of the combiner is monitored while the two other beams are blocked.

The AAS will manage the start-of-night alignment procedures for all ten beamlines with minimal human intervention. During this phase, it will ensure that the three axes of each beamline are co-linear to the required accuracy, using the DL/BCr axis as the reference axis. Intra-night correction of any subsequent alignment drifts will be handled by the AAS in the following manner. During stellar observations, we cannot measure any beam misalignment optically. We can however measure local temperatures around the optics that are the most likely culprits for inducing misalignment, i.e., mirrors M4 and M5. A software application will take these temperature readings as an input, predict how much the mirror angle has drifted, then output tip-tilt commands to the M4 and M5 mirrors to undo their expected angular drift at a rate of up to 1 Hz. Subsequent tilt and shear residuals will be optically sampled and corrected by the M4/M5 pair in between observations (every $\sim$30 minutes) by passing light from UTLIS through the beam train to BEASST. Every time UTLIS is switched on, the zero-point for FTT correction is updated to its current angle. This ensures that the stellar beam runs parallel to the UTLIS beam irrespective of angular drifts of the UTLIS beam. A shear between the UTLIS and stellar beams develops because UTLIS drifts angularly. This occurs because the stellar beam has a fixed pupil (i.e. the unit telescope primary mirror as imaged by the secondary mirror) whereas the UTLIS virtual pupil at the same plane as the telescope pupil drifts as a result of an angular drift of the UTLIS beam. This offset will be calibrated by BEASST once per hour. In this procedure, the telescope will be slewed to a bright stellar source that is close to the science or calibrator target. BEASST will record the offset between the stellar and UTLIS beam profiles arriving in the

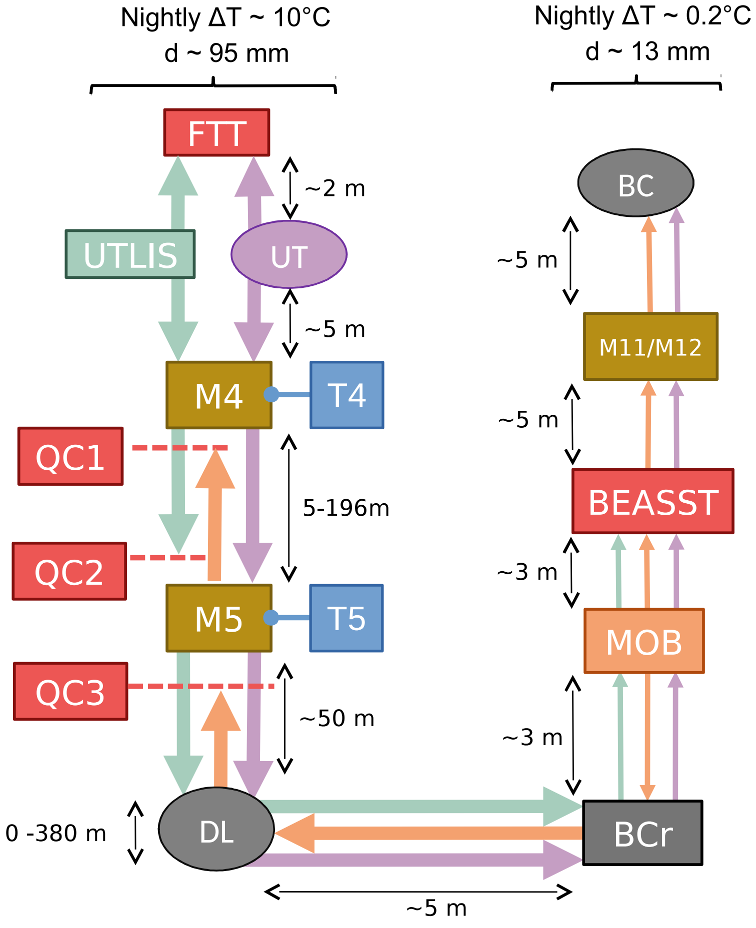

Figure 4: A single beamline at the MROI with its embedded alignment hardware. Core components of the beamline (gray and gold boxes) are defined in Figure 3. Light sources and their collimated beams are coloured in lilac (starlight), green (UTLIS) and orange (MOB). Red boxes denote optical beam alignment detectors. The FTT is the Fast Tip-Tilt system that actively corrects angular jitter of the stellar beam due to atmospheric turbulence. QC1, QC2 and QC3 are retractable large aperture photovoltaic quad cells for sensing the beam shear of any of the artificial reference sources. BEASST detects beam tilt and shear for reference sources and starlight. T4 and T5 are temperature sensors attached to mirrors M4 and M5 respectively.

beam combining laboratory. The AAS will then apply this offset when calculating shear corrections to make with the M4/M5 pair until the next such shear calibration.

Several components of the AAS are currently undergoing acceptance testing in laboratories at the University of Cambridge prior to integration at the MROI. The next Sections present a few early results for UTLIS and BEASST.

3. UNIT TELESCOPE LIGHT INJECTION SYSTEM (UTLIS)

3.1 Derived requirements

This source, one at each Unit Telescope, serves as a proxy for the stellar beam in the absence of a bright target. We have settled on the following requirements for this system:

- **Wavelengths**: visible for silicon-based detectors (FTT/QC) and for visual alignment; infrared for BEASST – Section 4 justifies why an infrared source is desirable for BEASST.
- **Beam diameters**: 25 mm to 50 mm (visible) and 50 mm to 70 mm (infrared) – These quantities are chosen as a balance between reducing intensity profile changes due to diffraction (larger beam desirable) and clear aperture constraints (smaller beam desirable).
- **Beam profile**: Diffracted profiles across full delay line stroke must be circularly symmetric (i.e., retain good wavefront quality) – The diffracted profiles arriving at BEASST evolve as the delay lines track, and so the presence of any asymmetric aberrations would cause systematic perturbations to BEASST measurements during intra-night correction procedures.
- **Photon rates and coherence**: $>6.4 \times 10^{13}\,\mathrm{s}^{-1}$ (visible, for QC, must be incoherent), $>1 \times 10^{15}\,\mathrm{s}^{-1}$ (visible, for visual alignment, can be coherent), $>8 \times 10^{10}\,\mathrm{s}^{-1}$ (infrared, for BEASST, must be incoherent) – These values stem from the predicted sensitivities of the QCs, BEASST and the human eye. In laboratory experiments we have found that interference effects provoke centroid perturbations when using coherent sources at a level incompatible with stabilizing beams as the sub-arcsecond level. Consequently, the beams used to measure alignment with BEASST and the QCs must be incoherent. Coherence is tolerable for coarse visual alignment tasks (i.e. viewing the beam on a card) that might happen seasonally.
- **Nightly angular drift**: $<12.4''\,\mathrm{K}^{-1}$ (95 mm space) – The alignment of the UTLIS beam will be set seasonally. Subsequently, its angular drift is compensated by regularly setting its angle as the zero point for FTT correction. A side effect of this is that the angular beam drift will effectively build up a shear offset between this source and that of the stellar pupil, and this growing offset is the origin of this requirement.

3.2 System design

The hardware for UTLIS is distributed between a cabinet in the UT enclosure and the Nasmyth Table attached to the UT. Optical functions performed in the cabinet are conducted fully in fiber to prevent optomechanical drifts from affecting performance. The Nasmyth Table assembly is shown in Figure 5. Taking inspiration from design choices made for the Fast Tip-Tilt system[8] at MROI for minimising drifts, the optomechanics are fabricated from aluminium, insofar as is possible. Aluminium's relatively high thermal conductivity allows temperature differences to equalise quickly.

Five functions are performed in sequence to produce a dual-wavelength collimated beam at the output of UTLIS:

1. **Light generation** – Light is generated at two wavelengths by two fiber-pigtailed superluminescent diodes (SLDs) that are coupled into single mode fibers (QPhotonics QSDM-1300-1 and QSDM-680-2). As per the requirements, these sources are temporally incoherent. By keeping the sources and their controllers in a cabinet, heat dissipation into the air of the enclosure is minimised.
2. **Wavelength combination** – The two wavelengths are connected via FC/APC mating sleeves (Thorlabs ADAFC4) to a Thorlabs WD6513F wavelength division multiplexer (WDM) that outputs the two beams in a single mode fiber.
3. **Transport from cabinet to Nasmyth Table** – The output of the WDM is connected to a 10 m long photonic crystal fiber (PCF) patch cable (NKT LMA-15-PM) via a FC/APC mating sleeve for transport from the cabinet to the Nasmyth Table.

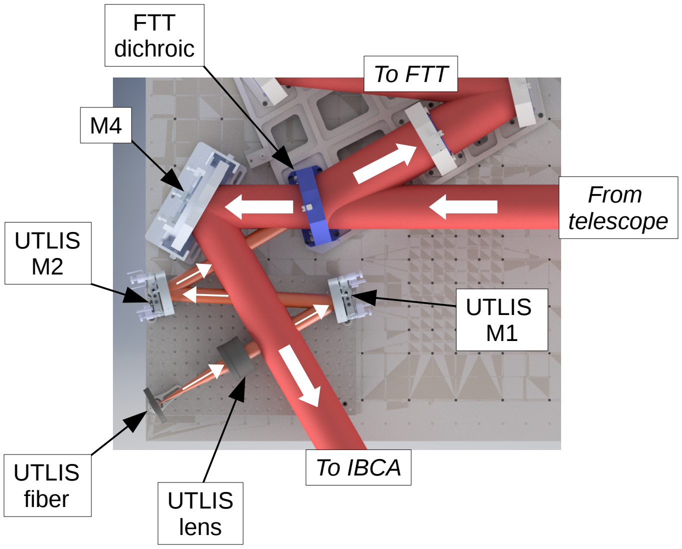

Figure 5: A birdseye view of UTLIS on the Nasmyth Table of the Unit Telescope. The device itself is located in the lower left corner. The small arrows show how the collimated light from UTLIS (orange beam) is coupled into the beam train via the dichroic splitter of the telescope's fast tip-tilt (FTT) system. In reflection, it travels to the beam combining laboratory. In transmission it passes to the FTT system. The path of the stellar beam (red) is marked by large arrows.

4. **Beam collimation** – On the Nasmyth Table, light emerges from the PCF in a cone. We are exploring two options for collimating the beam with a focal length around 380 mm. The first option is an aluminium-substrate, silver-coated off-axis parabola (Thorlabs MPD2151-P01). Alternatively, a collimating doublet lens been designed that is achromatic at the two wavelengths. It is also athermalised[9] using a combination of glasses (N-LAK12 and SF57HTULTRA) that permits the focal length of the lens to vary with temperature to counteract the expansion of the aluminium baseplate on which the Nasmyth optics sit. This option is more expensive and will take several months to manufacture, but is more tolerant of misalignment. Currently we are practically investigating the performance and feasibility of the off-axis parabola (OAP) for producing a collimated beam. If it does not seem viable we will order the lens instead.

5. **Injection into MROI beamline** – The parallel UTLIS beam is then injected into the MROI beamline at the FTT dichroic. Fine tilt/shear adjustment is made possible by a pair of flat silver-coated mirrors (Thorlabs PF30-03-P01) in Newport Ultima U300 mounts that are steered using piezo inertia actuators (Thorlabs PIA13).

3.3 Laboratory performance verification

A partially complete version of UTLIS has been assembled in our laboratory in Cambridge for optical testing. At the time of writing we have received both SLDs as well as the WDM, PCF, OAP and various optomechanics. Unfortunately we have not received controllers for the SLDs yet. In the interim, the infrared SLD is being operated with a current-limiting resistor. The visible SLD requires temperature stabilisation, so we have decided not to operate it until its controller arrives and instead we have used a laser diode (Thorlabs HL6312G) as a 635 nm substitute. Its light has been injected directly into the visible port of the WDM using a pair of steering mirrors and a lens. As such, its flux is expected to be lower than that of the fiber-pigtailed SLD that is proposed in the design. When driven below its lasing threshold, the laser diode is partially coherent but dim. However when driven above its threshold it is coherent and bright. This is less convenient than the SLD, which can be

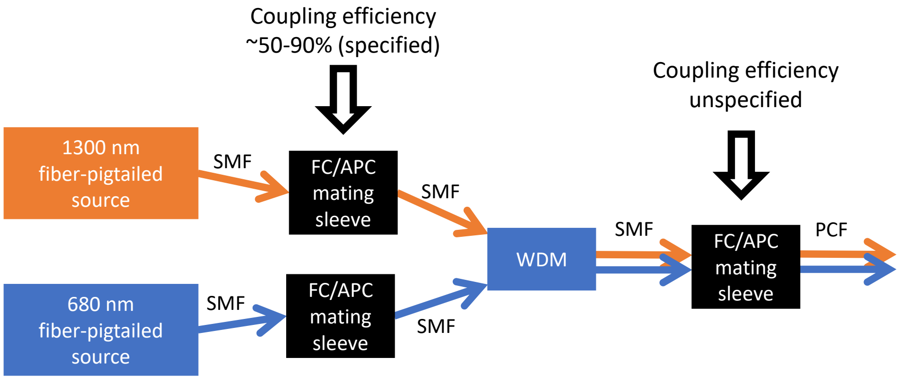

Figure 6: Our adopted fiber-based strategy for combining the visible and infrared sources of UTLIS in a cabinet, then injecting them into a photonic crystal fiber (PCF) for transport to the Nasmyth Table. The visible and infrared wavelengths are generated by fiber-pigtailed sources. Each of these fibers is then connected by a FC/APC mating sleeve to a wavelength division multiplexer (WDM) that combines the two inputs in fiber. The output of the WDM is then joined to a connectorised PCF by another FC/APC mating sleeve. The coupling efficiency at the SMF/PCF butt joint will have to be measured and optimized for each installation.

simultaneously incoherent and bright as demanded by the requirements. A small number of tests have been performed so far to validate the performance of this design with respect to throughput and beam diameter.

3.3.1 Throughput

The strategy for combining light from the two sources of UTLIS and coupling them into a photonic crystal fiber (PCF) is outlined schematically in Figure 6. Compared with a free-space coupling method, which might be based around a dichroic splitter, this solution requries no manual beam alignment and is immune to beam wander as a function of temperature changes.

Two key issues arise from this strategy:

- **Mode filtering** – The WDM uses an optical fiber (SMF-28E) for which the single mode cut-off is at an infrared wavelength. As a consequence, the visible output of the WDM contains multiple spatial modes. Fortunately, the PCF filters the output to a single mode, which suppresses any effects due to potentially time-varying interference between multiple spatial modes. However, this is a lossy process since only a small amount of flux is transported at the fundamental mode. A laboratory experiment was necessary to confirm the amount of flux that could be injected using a practical system.
- **Coupling between WDM and connectorised PCF** – Connectorised PCF patch cords are hermetically sealed at both ends to prevent moisture and dust from entering the capillaries that form the waveguide. This is done by collapsing the capillaries at a distance of approximately 150 µm from the end of the fiber. In this collapsed region, the PCF no longer guides light; beams expand in glass for 150 µm prior to the air interface. While at first this seems problematic for butt coupling, one realises that the PCF mode field diameter (MFD) is larger than that of the SMF, so in fact it might be beneficial for the beam to expand

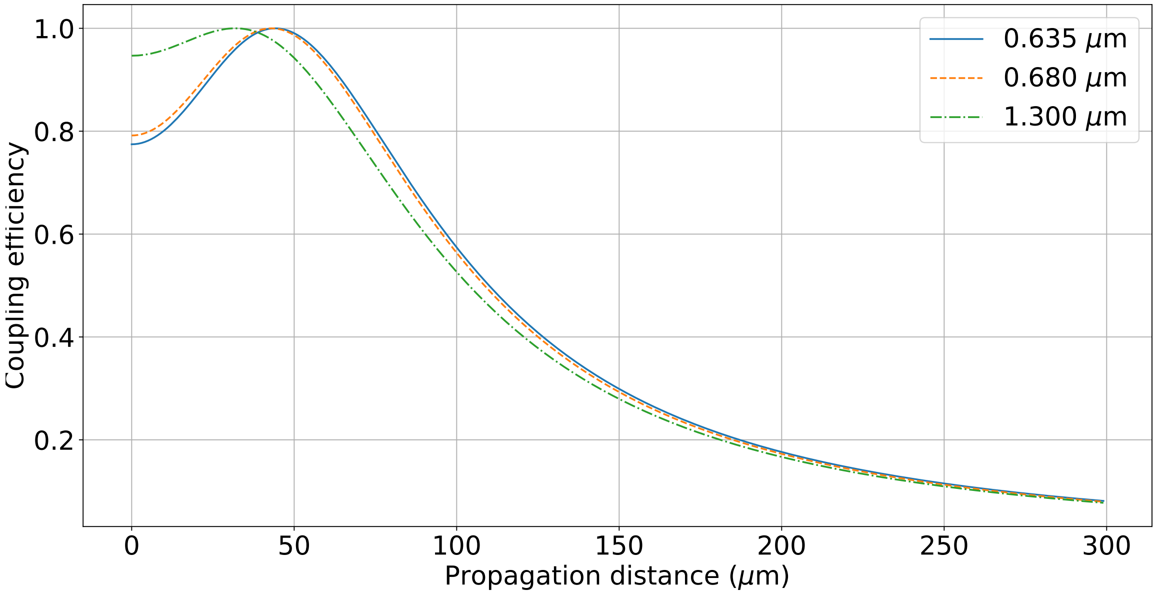

Figure 7: Predicted coupling efficiency against propagation distance for butt coupling between a single mode fiber (SMF-28E) and a collapsed photonic crystal fiber (NKT LMA-15-PM). The propagation distance is the length of the collapsed region of the PCF. The behaviour for three wavelengths is plotted. These correspond to the experiments reported here (0.635 µm and 1.300 µm) and to the final system design (0.680 µm and 1.300 µm) we intend to utilize. The coupling efficiency at the nominal end cap distance (150 µm) is expected to be approximately 30% for the three wavelengths.

by a small amount between the WDM and the PCF. Figure 7 shows the coupling efficiency predicted for such an interface from the equation*

$$\alpha_{butt}(dB) = -20 \log_{10} \frac{2\,\omega_{PCF}\,w(z)}{\omega_{PCF}^2 + w(z)^2}\ , \tag{1}$$

where ω_{PCF} is the mode field diameter of the PCF and $w(z)$ is the diameter of the diverging beam that has arrived at the PCF from the SMF,

$$w(z) = \omega_{SMF}\sqrt{1 + \frac{\lambda z}{\pi \omega_{SMF}^2}}\ . \tag{2}$$

Here ω_{SMF} is the mode field diameter of the SMF at wavelength λ and z is the length of the end cap. The length of the collapsed region in NKT's LMA-15-PM PCF patch cable is not specified, so the practical loss arising from this method of coupling is uncertain.

In view of this uncertainty, we have performed laboratory experiments to quantify the losses in our proposed configuration. A FC/PC socket was attached directly to a Raptor Owl Mini InGaAs camera into which connectorised optical fibers could be plugged. The tip of each fiber was close enough to the focal plane array that the expanding beam underfilled the sensor. For each readout, the photon flux (photons arriving per second) was recorded as the sum of the values of illuminated pixels minus a dark background, divided by the integration time and multiplied by the manufacturer-specified pixel gain (photoelectrons per analog-to-digital unit). This was then scaled to accommodate the quantum efficiency at the two respective wavelengths. Several variants of the experiment were carried out:

---

*`https://www.thorlabs.com/images/TabImages/Application_note_-_stripping_cleaving_and_coupling.pdf`

No.	λ **(nm)**	**Experiment**	**Photon flux** (s^{-1})	**Coupling efficiency (relative to No.)**
1	635	WDM (below)	1.2×10^{10}	1.00 (1)
2	635	WDM + PCF (below)	1.7×10^{8}	0.01 (1)
3	635	WDM + Reversed PCF (below)	6.4×10^{8}	0.05 (1)
4	635	WDM (above)	3.9×10^{12}	1.00 (4)
5	635	WDM + PCF (above)	4.0×10^{10}	0.01 (4)
6	1300	SLD	1.3×10^{13}	1.00 (6)
7	1300	SLD + WDM	1.2×10^{13}	0.92 (6)
8	1300	SLD + WDM + PCF	7.8×10^{11}	0.06 (6)
9	1300	SLD + WDM + Reversed PCF	1.8×10^{12}	0.14 (6)

Table 1: Observed photon rates and coupling efficiencies for a butt-coupled SMF/photonic crystal fiber interface. For experiments that used the laser diode at 635 nm, the labels "below" and "above" refer to whether it was operated above (coherent) or below (incoherent) its lasing threshold. In the rightmost column, the number in parentheses indicates the measurement to which the coupling efficiency is referenced.

- An infrared superluminescent diode (QPhotonics QSDM-1300-1, centre wavelength 1.3 μm, maximum power 0.2 mW) was driven at an unknown optical power below its maximum rating. Its flux was measured at the output of the:
  - SMF from the SLD.
  - WDM, having been interfaced with the SLD fiber output.
  - PCF, having first been interfaced with the SLD fiber output, then the WDM.
- A visible laser diode (Thorlabs HL6312G, centre wavelength 635 nm, maximum power 5 mW) was driven in some cases above and in some cases below its lasing theshold. Its flux was measured at the output of the:
  - WDM, having been coupled from free space
  - PCF, with light having been coupled from free space into the WDM, then from the WDM to the PCF.

Table 1 summarises the absolute photon fluxes and coupling efficiencies determined from our measurements. Experiment numbers 8 and 9 reveal that the infrared source will comfortably meet its photon flux requirement of $7.5 \times 10^{10}\,s^{-1}$ at the output of UTLIS. Experiments 2, 3 and 5 indicate that the visible source used here falls far short of meeting its requirement for photon flux. However we believe that the photon rate produced by the fiber-pigtailed SLD will be orders of magnitude greater than has been achieved by the interim laser diode that we used in this experiment.

For both sources, the coupling efficiencies were lower than expected from the model plotted in Figure 7. Interestingly the efficiency depended on which end of the PCF was mated with the WDM. When the PCF was reversed, a large gain in efficiency was observed. For the visible source, the efficiency ranged between 1% (Experiment 2) and 5% (Experiment 3). For the infrared source it ranged between 6% (Experiment 8) and 14% (Experiment 9). Both of these are much lower than the 30% expected from the model. It may be the case that there are large variations in the length of the collapsed region in the PCF. For future beamlines it will be important to test each PCF in the laboratory before it is deployed at the MROI. Another experiment that was tried was to see if there was a difference in coupling efficiency between a coherent (laser diode driven above its lasing threshold – Experiments 1, 2 and 3) and incoherent source (laser diode driven below its lasing threshold – Experiments 4 and 5) at the same wavelength. No significant difference was observed.

Our tests were also able to investigate the stability of the system throughput at the visible wavelength as the balance of modes within the WDM fluctuated. This fluctuation is driven by changes in path length and

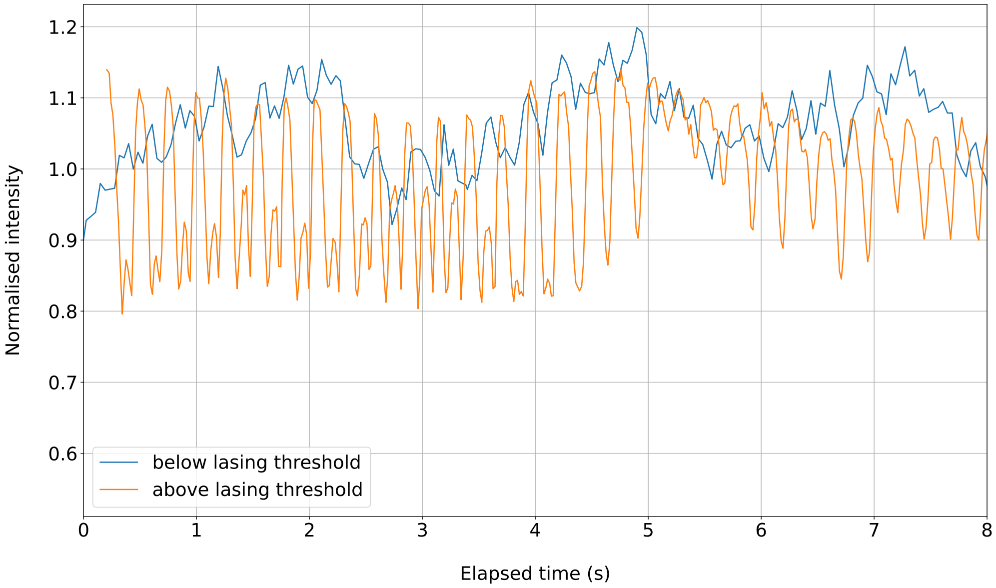

Figure 8: Fluctuations in the intensity of visible light emitted from the PCF when coupled with a WDM. The two datasets correspond to the Thorlabs HL6312G laser diode being driven below and above its lasing threshold, for which the light is temporally incoherent and coherent, respectively.

bending of the fiber. To investigate this the output of the PCF was monitored at ∼30 Hz by a Raptor Owl Mini as the WDM was oscillated by hand with an amplitude of a few centimeters. Figure 8 shows results for the cases of (a) the laser diode being driven below its lasing threshold and (b) being driven above its lasing threshold. The amplitude of intensity fluctuations was about ±20% in both cases. We anticipate that similar amplitude variations would be observed as a function of temperature as the WDM expands and contracts in length, but at a much slower rate. It is possible that this fluctuation could lead to biases in alignment detection if the coupled flux is low and close to the detection limit. A mitigation strategy could be to run a loop that adjusts the current supplied to the source to hold the output power constant in the presence of such fluctuations.

3.3.2 Beam diameter

To assess the nature of the coupled PCF beam, the light emerging from it was projected onto a paper screen printed with dimensioned concentric circles. A C-mount photographic lens was fitted to a hyperspectral InGaAs camera (Raptor Owl Mini) and was focussed on the screen to capture images of the visible and infrared intensity profiles. Figures 9a and 9b show the Gaussian-like beam profiles observed by this method for the visible and infrared sources, respectively. Lower bounds on the beam diameters at a distance of 381 mm (the focal length of the collimating optic) were 25 mm for $\lambda = 635$ nm and 60 mm for $\lambda = 1300$ nm. These results are close to the predicted values from the Gaussian beam expansion equation where the beam waist is set as the mode field diameter (i.e. 55 mm for $\lambda = 1300$ nm, 25 mm for $\lambda = 635$ nm).

Interestingly, when the visible beam was viewed on a card a few centimeters from the output of the PCF, the intensity profile resembled a bright hexagon-like central lobe surrounded by six dim circular satellites (see Figure 10). This property has been modelled in the literature[10] and that analysis suggests that the hexagon rotates by $\pi/6$ in the transition between the near and far fields. In future work, it would be worth incorporating these findings into a propagation code to ensure that this behaviour will not disturb any of the QC or BEASST beam alignment measurements.

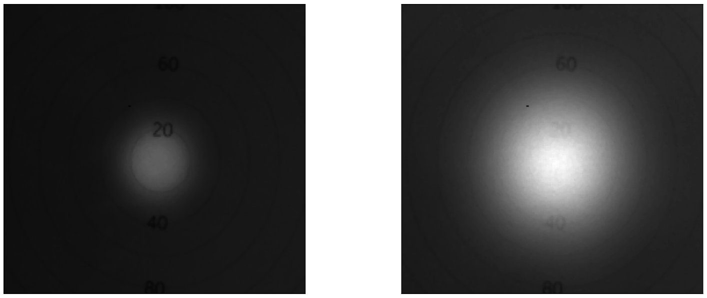

(a) λ =635 nm (b) λ =1300 nm

Figure 9: Beam profiles emitted from the NKT LMA-15-PM fiber viewed on a screen 381 mm away from the PCF tip. This distance corresponds to the focal length of the collimating optic. Concentric circles are printed on the screen and dimensioned in millimetres. The scale within these images is identical, so it is clearly noticeable that the diameter of the infrared beam is larger than that of the visible beam.

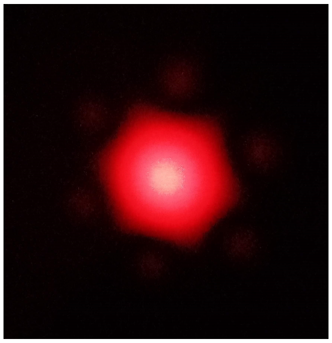

Figure 10: Intensity distribution of λ=635 nm light emitted from the PCF, as viewed on a white card held a few centimeters from the output. Note the bright, hexagonal central lobe and six dim, circular satellites.

4. BEAM TILT AND SHEAR DETECTION BY BEASST

4.1 Derived requirements

This sensor, one for each of the beamlines associated with a Unit Telescope, must measure the tilt and shear of its beam as it arrives in the beam combining laboratory. We have settled on the following requirements for BEASST:

- **Spectral sensitivity**: >1.1 µm – Once per hour on an observing night, BEASST will calibrate the difference in shear between the stellar beam and the UTLIS beam. When viewing stellar light, we must consider the effect of differential atmospheric refraction.[11] For a star at a zenith angle of 60°, the difference in angle between its beam at 0.6 µm (the lower end of the MROI's spectral range) and 1.7 µm (the sensitivity cut-off for InGaAs detectors) is approximately 1″ on sky. This is amplified by a factor of $14.7 \times 7.3 \times 6 \approx 640$ by the time it reaches the detector plane of BEASST. Each UT at the MROI will be fitted with an atmospheric dispersion corrector (ADC) that will largely eliminate this relative angle. For now we assume that residuals of this correction will be at the level of 0.2% of the relative angle (i.e. ∼1″ at BEASST). The shear between beams at the two extremes of the band measured at BEASST is a function of the path length and angle. Each stage of beam compression at the MROI amplifies the angle, so we split the calculation of shear into contributions while the beam is of fixed diameter (i.e. 630 m at 95 mm, 5 m at 13 mm, 0.2 m at 2.2 mm). If the full band from 0.6 µm to 1.7 µm was passed to BEASST, the shear between beams at the extremes of the band would take up ∼15% of the beamline intra-night error allowance. This cannot be accommodated because there are many other error contributions to consider. Differential refraction is much more severe at visible wavelengths than infrared wavelengths. If we remove visible wavelengths (i.e. reduce the band to 1.1 µm to 1.7 µm), the differential refraction angle between the band edges is 0.2″ on sky. This gives a much more manageable shear error at BEASST of 3% of the beamline allowance.
- **Clear aperture**: >25.3 mm – BEASST samples beams in the beam combining laboratory where the beam diameter is nominally 13 mm. In reality, the largest possible diameter (22 mm) is given by a stellar beam that has been disturbed by atmospheric turbulence and propagated over the longest beam path (>600 m). To allow for misalignment in this extreme case, the clear aperture is defined to be 15% larger than this diameter.
- **Measurement accuracy**: 0.44″ for tilt and 42 µm (reference sources) or 76 µm (starlight) for shear – The accuracy of BEASST's measurements depends on centroid noise, any thermal drift of its optomechanical components ($\Delta T \sim 0.2\,^{\circ}$C) and other systematics. Note that these values apply in two axes (i.e. for a single axis the requirement would be a factor of $\sqrt{2}$ more precise).
- **Dynamic range**: > ±20″ in tilt, > ±2 mm in shear – BEASST is intended to be a fine alignment diagnostic. These values are ten times more than the alignment error budget allocations during the start-of-night and intra-night procedures.
- **Power dissipation**: <2 W per unit – Heat dissipation inside the beam combining laboratory is limited to preclude the formation of air currents around the beam paths. BEASST must not significantly add to the heat input.

4.2 System design

Figure 11 shows the optomechanical design for BEASST. It picks off ∼2.5% of the incoming beam intensity, using a custom broadband antireflection coating on the front and back sides of a Suprasil window that will intercept the beam at a 15° angle of incidence. The beam size will then be reduced by a factor of 6 (Thorlabs BE06R/M) to underfill a custom-built Shack-Hartmann sensor sensitive at wavelengths between 1.1 µm and 1.7 µm (Raptor Owl 640, Edmund Optics 21-147, Thorlabs FELH1100). As the camera is specified to consume 4 W of power, it will be enclosed in a thermally insulated box that dissipates heat to an external area rather than the beam combining laboratory. The power dissipation requirement also means that the device cannot be directly connected to a computer inside the laboratory. We have chosen to interface the camera via GigE, which allows remote operation

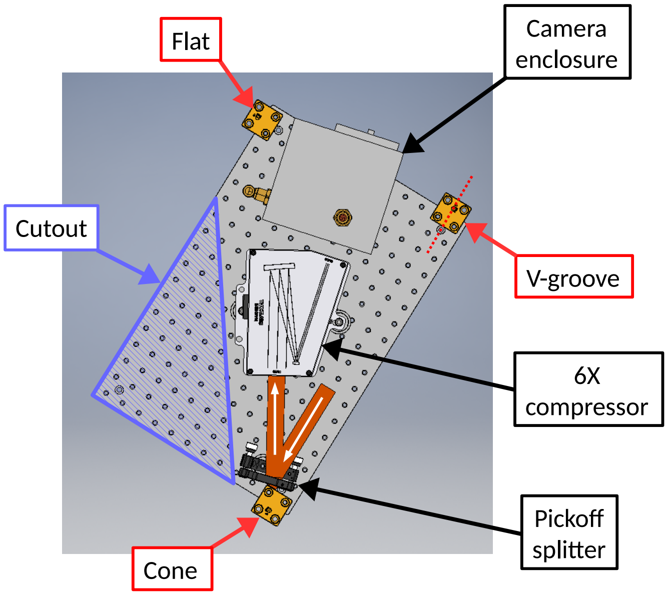

Figure 11: A birdseye view of the optomechanical design for BEASST. The beam arriving from the UT, UTLIS or MOB is shown in orange and strikes a pickoff splitter. The transmitted beam travels onwards to the beam combiner while the reflected beam first enters a beam compressor before arriving at a Shack-Hartmann sensor inside a thermally-insulated box. The aluminium baseplate is kinematically mounted in order to interface with the stainless steel optical bench.

at distances up to 100 m. GigE is also convenient for multiplexing the ten BEASST cameras as we can utilise the existing network infrastructure of the interferometer. This assembly must be insensitive to local thermal fluctuations. The pickoff splitter, compressor, Shack-Hartmann sensor and insulated box sit on an aluminium baseplate (Thorlabs MB3045U/M). This matches the materials for the pickoff splitter and compressor mounts to avoid creeps due to differences in coefficient of thermal expansion. A kinematic interface between BEASST and the stainless steel optical table that it is mounted on will allow the aluminium baseplate to freely expand and contract. In this way angular drifts due to warping are avoided. An unused section of the baseplate is cut out in order to bring the centre of mass of the assembly closer to the centre of the area enclosed by the kinematic interfaces. This distributes the load more evenly amongst the three interfaces. It also reduces the footprint of the assembly.

BEASST is unconventional because, enabled by its Shack-Hartmann (SH) sensor, it can measure beam shear and tilt with a single measurement. Conventional alignment sensors must determine these parameters with two separate measurements, either by using two separate detectors or by reconfiguring the optics in front of a single detector. Compared with these options, BEASST saves money (only one expensive camera is required instead of two) or time (shear and tilt are measured simultaneously without needing to switch configuration). BEASST measures beam tilt by observing the average displacement of the SH spots. Beam shear is measured by processing the images in a few steps. First, the image is divided up into boxes that contain no more than one SH spot. Next, the flux within each box is summed. The summed flux is assigned coordinates for the centre of its associated microlens. In effect, this reduces the SH spot array to one in which each pixel is as wide as a microlens. The centroid of the resulting intensity profile determines the beam position.

4.3 Laboratory performance verification

A partially complete version of BEASST has been assembled in our laboratory in Cambridge. Two substitutions have been made for this phase of testing. The first is that we are using a Raptor Owl Mini instead of a Raptor

Owl 640 as the focal plane array for the SH sensor. The sensor dimensions are equal. The only difference is that the 640 is thermo-electrically cooled to 15 °C while the Mini is uncontrolled in temperature. The background for the Mini is therefore much higher than for the 640, particularly if it is operated on a hot day. The second substitution regards the custom pickoff splitter. For now we are using an uncoated Suprasil window (Edmund Optics 15-472), which was available quickly and cheaply off the shelf. It is expected to give a 10% reflection to BEASST instead of the required 2.5% while we await the manufacturing of a custom splitter. UTLIS has been assembled concurrently, and offers a convenient source of collimated light with which to test BEASST.

4.3.1 Tilt measurement linearity

We devised an experiment to compare the tilt measurement of BEASST with a conventional tilt sensor comprised of a lens (f=200 mm) and a CMOS focal plane array (Basler acA-1280-60gm). Since this is a visible-sensitive sensor, a visible wavelength was chosen for the beam passed to both detectors. Since UTLIS was already set up for its own experiments, we decided to use its visible light (λ=635 nm) to illuminate the two alignment detectors. The beam that UTLIS outputs is much larger than the clear aperture of BEASST. To allow the beam to underfill BEASST, we assembled a 7.3× Galilean beam compressor (Comar Optic 1000 PQ 63 and 160 NQ 25) to reduce the size of the UTLIS beam by the same factor as the compressor installed at the MROI. To ensure that UTLIS provided an adequate level of flux for this experiment, light from its laser diode was injected directly into the PCF, bypassing the WDM. The collimated beam exiting the compressor was steered towards the BEASST pickoff splitter. The reflected beam was passed via the 6× compressor to the Shack-Hartmann array, while the transmitted beam proceeded to the conventional tilt sensor. The laser diode was driven below its lasing threshold to prevent the front and back surface reflections from the pickoff splitter from interfering with each other and disturbing tilt measurements. A 1-inch diameter mirror was mounted in a Newport Agilis AG-M100N piezo-actuated mount in order to apply sub-arcsecond tilts to the beam just before it reached the BEASST pickoff splitter. In this way, we simultaneously measured the response of BEASST and the conventional sensor to a common applied beam tilt. The experiment was carried out on a particularly hot day in a lab that is not temperature controlled. Accordingly, the dark current in the two detectors was noticeably elevated. In addition, laboratory seeing played a role. While watching the image stream from the conventional sensor in real time, the spot was obviously moving position at a frequency faster than 1 Hz. The combined noise from laboratory seeing and an elevated detector dark current was mitigated by averaging 30 images for each measurement.

Figure 12 shows a preliminary dataset of the tilt measured by BEASST against the tilt measured by the conventional tilt sensor. These data are plotted alongside a unity slope. Broadly speaking, the BEASST tilt measurement agrees in scale with the conventional method. This tells us that the scaling factors for beam compression and microlens array focal length that have been applied correctly when processing the BEASST images. Error bars have been estimated by calculating the standard deviation of tilt measurements when the beam was nominally stationary. These were $0.51''$ and $0.72''$ for BEASST and the conventional sensor, respectively. The noise for BEASST in this experiment lies a little outside its requirement of $0.44''$. We note that residuals of seeing and dark current might have raised the noise floor in spite of averaging 30 images per measurement. While the tilt response of BEASST appears to be parallel to the unity slope, the vast majority of points lie above it. This observation is not yet understood.

The median photon rate in these experiments was $3.3 \times 10^8\,\mathrm{s}^{-1}$. This value was obtained by summing the counts in illuminated boxes, dividing by the exposure time (1 ms) then multiplying by the manufacturer specified electron gain ($0.71\,e$/DN) and quantum efficiency. When BEASST is installed at MROI, only 0.014% of the flux exiting UTLIS will arrive at its focal plane array. This corresponds to a photon rate of $7.5 \times 10^{10}\,\mathrm{s}^{-1}$ $\times 0.014\% = 1.1 \times 10^7\,\mathrm{s}^{-1}$. In future experiments we will reduce the flux of the light source to validate the performance of BEASST under more realistic conditions.

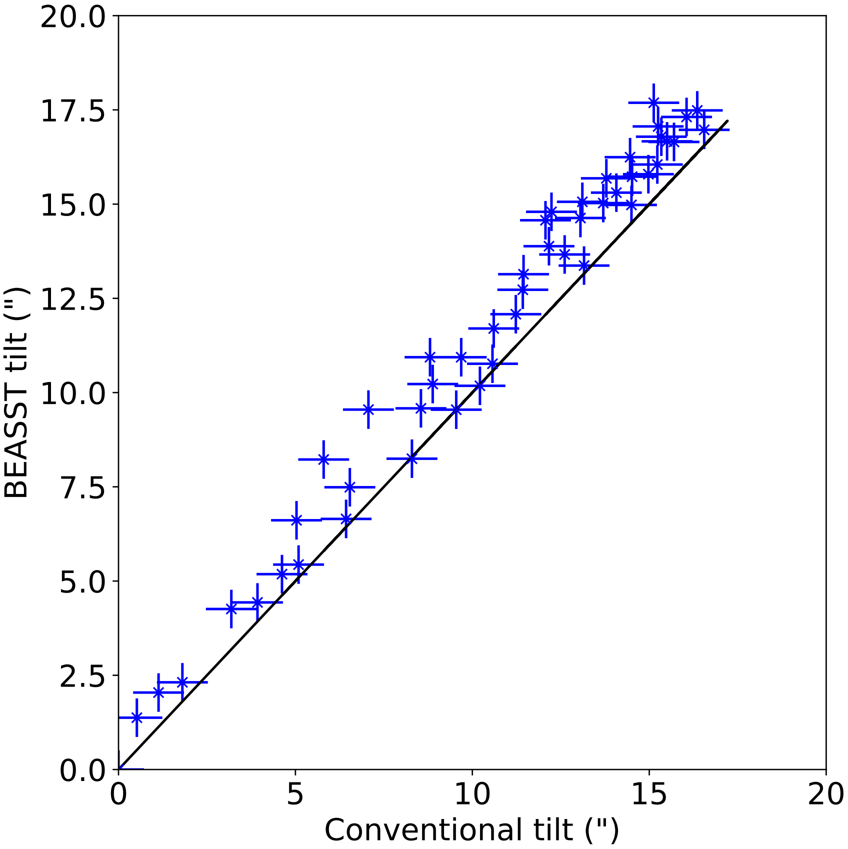

Figure 12: Tilt measured by BEASST plotted against tilt measured by a conventional detector as the angle of the incoming beam was adjusted in sub-arcsecond steps. The error bars correspond to the jitter in the tilt measured by the respective detectors while the beam was stationary.

5. NEXT STEPS

We hope that the items that have not arrived yet will soon be in hand so that meaningful laboratory tests can go ahead.

For BEASST we wish to validate the following:

- **Measurement linearity** – This test would improve on the experiment presented in Section 4.3.1. To combat high levels of dark current observed in the first iteration of the experiment, the next iterations should be carried out in a cooler environment. To reduce the impact of laboratory seeing on alignment masurements, the beam path could be shielded by cardboard panels, for example. The range of the experiment should be expanded to $\pm 20''$ to validate the derived requirement for this system. Following this, we will reconfigure the setup to explore the dynamic range of the shear measurement. The shear of the incoming UTLIS beam could be controlled by mounting a mirror that deflects light towards BEASST on an actuated linear slide. This would allow the beam shear to be adjusted in $\sim 10\,\mu\text{m}$ steps in the horizontal plane. The conventional tilt detector could be reconfigured to a shear detector simply by removing the lens that lies in front of its camera.
- **Drift in tilt and shear measurements** – This experiment will quantify how the measured values of tilt and shear drift even when the beam under observation is stationary. It will be carried out in a laboratory where the air temperature varies by several °C diurnally. A collimated beam could be passed to BEASST,

but this would require a number of optics that could themselves drift. A more robust method is to directly illuminate the BEASST pickoff splitter with a beam emitted from a single mode fiber placed ∼1 m away. The wavefront of this beam would be quasi-spherical with a radius of curvature of 1 m. We will observe how individual SH spot centroids drift with temperature, which relates to the drift in measured tilt. Since the emitted wavefront is spherical, angular drifts of the fiber axis would not cause beam tilt to be registered by BEASST. If the fiber tip moved laterally, BEASST would measure a negligbly small tilt shift.[12] Similarly, the drift in shear can be observed by passing the spherical beam through a pinhole en-route to BEASST. For a certain pinhole size, the beam that arrives at BEASST will underfill its clear aperture, allowing the shear measurement to be monitored in the presence of temperature fluctuations. This would likely place an upper limit on BEASST's drift because the pinhole itself might move laterally by ∼10 µm with temperature.

- **Sensitivity at required flux level** – We are interested in the sensitivity of BEASST's tilt and shear measurement in the presence of random noise sources, such as detector dark current and readout noise. We will pass a collimated beam to BEASST and capture a large sample (N>200) of BEASST images. The standard deviation of the extracted tilt and shear indicates the effect of random noise on these measurements. As a minimum, the sensitivity should be measured at the discrete flux level provided by UTLIS. If time permits it would be helpful to repeat this experiment over a range of fluxes to enhance our understanding.

For UTLIS we wish to validate the following:

- **Photon flux provided by visible SLD** – This will be a repeat of the experiment described in Section 3.3.1 to test the visible SLD that we have not yet been able to operate safely.
- **Beam profile after tens of metres of propagation** – In this experiment, UTLIS will be installed at the COAST bunker, located a short drive outside Cambridge. Its delay lines and retroreflecting carts provide a variable optical path delay of up to ∼80 m. The UTLIS beam will be set up to align its light coaxially with the delay line. A paper screen will be placed at a fixed location in the return beam from the retroreflecting cart. The screen will be observed by an imaging camera, as in Section 3.3.2. By moving the cart, we can observe how the beam profile changes with distance without having to relocate the imaging equipment for each measurement. Following on from this experiment, we will install BEASST to capture the beam returning from the cart. As in Section 4.3.1, a 7.3× beam compressor will be installed so that the UTLIS beam underfills the clear aperture of BEASST by the same factor as at the MROI. With BEASST we will measure the tilt and shear of the beam as a function of propagation distance. Ideally these will remain constant. If not, this could indicate that either (a) the UTLIS beam is not perfectly aligned with the delay line axis, or (b) wavefront error in the UTLIS beam is perturbing BEASST's measurements of tilt and shear. This end-to-end test is intended to validate the performance of a subset of the AAS, not just its individual components. Seeing induced by propagation over long path lengths could be an additional noise source in this experiment. However we expect the air inside the bunker to be very stable, since footfall inside the area is low and very few heat sources are present.
- **Angle and focus drift with temperature** – This experiment will be carried out in a laboratory in which the air temperature fluctuates by several °C diurnally. The output beam of UTLIS will be passed directly to BEASST (i.e. without its pickoff splitter or compressor) so that its tilt can be measured over time. We expect that the angular drift of UTLIS will be much larger than the tilt measurement drift of BEASST. Simultaneously, we can monitor the drift in focus of the UTLIS beam because this would manifest as a change in the average spacing between SH spots.[12] One concern is that the surface of the stainless steel optical table on which UTLIS and BEASST are mounted might warp due to temperature changes. This would add a component of tilt drift that is not related to UTLIS. Care must be taken when interpreting the results of this experiment.

6. CONCLUSION

This paper has presented the current status of the Automated Alignment System for the Magdalena Ridge Observatory Interferometer. We have described some encouraging results from early tests of advanced versions of a collimated reference beacon (UTLIS) and a beam shear and tilt detector (BEASST). A list of factory acceptance tests has been outlined for verifying the performance of these components against their derived requirements. Full validation will only be possible once a few pieces of delayed equipment have arrived in our laboratory. The beam profile and drift tests involving UTLIS are of highest priority because, depending on the measured performance, we may choose to replace its collimating off-axis parabola with a custom doublet lens that will take up to 20 weeks to manufacture. Initial results from experiments with BEASST are close to meeting requirements, and we believe that it will be possible to meet them if environmental conditions in the laboratory are improved.

ACKNOWLEDGMENTS

This material is based on research sponsored by Air Force Research Laboratory (AFRL) under agreement number FA9453-22-2-0040. The U.S. Government is authorized to reproduce and distribute reprints for Governmental purposes notwithstanding any copyright notation thereon.

REFERENCES

[1] Goodman, J. W., [*Introduction to Fourier Optics*], McGraw-Hill, New York, USA (1996 (second edition)).

[2] Horton, A. J. et al., “Diffraction losses in ground-based optical interferometers,” *MNRAS* **327**, 217–226 (2001).

[3] Luis, J. J. D. et al., “Augmented design for a fully automated alignment system at the magdalena ridge observatory interferometer,” *Proc. SPIE* **10701** (2018).

[4] Luis, J. J. D. et al., “Deployment of beam alignment hardware at the magdalena ridge observatory interferometer,” *Proc. SPIE* **11446** (2020).

[5] Buscher, D. F. et al., “The conceptual design of the Magdalena Ridge Observatory Interferometer,” *Journal of Astronomical Instrumentation* **2**(2) (2013).

[6] Mortimer, D. J. et al., “First laboratory results from FOURIER, the initial science combiner at the MROI,” *Proc. SPIE* **11446** (2020).

[7] McCracken, T. M. et al., “The MROI fringe tracker: laboratory tracking with ICONN,” *Proc. SPIE* **9146** (2014).

[8] Young, J. S. et al., “The performance of the MROI fast tip-tilt correction system,” *Proc. SPIE* **9146** (2014).

[9] Schwertz, K., Dillon, D., and Sparrold, S., “Graphically selecting optical components and housing material for color correction and passive athermalisation,” *Proc. SPIE* **8486** (2012).

[10] Mortensen, N. A. and Folkenberg, J. R., “Near-field to far-field transition of photonic crystal fibers: symmetries and interference phenomena,” *Optics Express* **10**(11), 475–481 (2002).

[11] Roe, H. G., “Implications of atmospheric differential refraction for adaptive optics observations,” *Publications of the Astronomical Society of the Pacific* **114**, 450–461 (2002).

[12] Chernyshov, A. et al., “Calibration of a Shack-Hartmann sensor for absolute wavefront measurements,” *Applied Optics* **44** (2005).